sion-recovery technique (T1 IR) under proton-noise-decoupling conditions. A waiting time of 140 s was maintained. Every run consisted of at least 48 accumulations at 10 different pulse intervals. The samples were stored in 12-mm tubes, degassed by at least two freeze-pump-thaw cycles, and sealed under a nitrogen atmosphere. All measurements were carried out in duplicate at 293 ± 2 K. Finally, the T_1 values were obtained by using a fitting program.[37] The standard deviation is approximately 10%.

Nuclear Overhauser enhancement factors were measured for all crown ethers by using the standard ALNOE pulse sequence. Whenever it was necessary for the assignment of the resonances, 2D (^{13}C, ^{1}H) correlated spectra were recorded.

Molecular Mechanics. The molecular mechanics method determines the steric energy of conformations of a molecule as a measure of their relative stabilities. The steric energy is a sum of bonded (stretch, bend, stretch-bend, and torsion) and nonbonded (van der Waals and electrostatic) contributions.

Steric energies of conformations of the macrocyclic polyethers were minimized with the MM2 force field.[21] Parameters for the energy functions were standard ones, except for the aromatic moieties. Following a communication by Allinger,[38] the parameters involving aromatic carbon atoms were modified.[39] In one instance calculations were also carried out with MMP2,[40] the MM2 program for conjugated systems: the relative energies agreed within 0.1 kcal mol^{-1}. The parameters for the xylyleno and benzo moieties therefore are assumed to give reliable results. For the pyrido moiety, however, parameters involving the aromatic nitrogen atom were not available and had to be estimated,[39,41] and they are thus less reliable. In all cases the error in the results is assumed to be less than 1 kcal mol^{-1}.

Starting conformations for the energy minimization of the macrocycles investigated were obtained from X-ray coordinates or were generated by molecular graphics methods with the aid of CPK models. In this way local minima are found for the steric energy in conformational space. Macrocycles with ring sizes of 18 atoms or larger, however, have hundreds of local minima,[42] and the substituents even enlarge this number. A systematic search for the global minimum is therefore not feasible, and at most it can be rationalized that certain conformations are of low energy, e.g., conformations that have all macrocyclic C-C dihedrals gauche ($g^+ = 60°$ or $g^- = -60°$) and all C-O dihedrals anti ($a = 180°$),[42] which means that their torsion code consists of ag^+a and ag^-a units.

T_1 Data. The spin-lattice relaxation times are collected in Tables I-IV. Abbreviations used are nd, not determined; bz benzylic; rest, the average of the remaining macro ring carbons.

Acknowledgment. We thank J. M. Visser and J. L. M. Vrielink for performing the T_1 measurements. Use of the service and facilities of the Dutch CAOS/CAMM Center, under Grants SON-11-20-700 and STW-NCH-44.0703, is gratefully acknowledged. This investigation was supported by the Netherlands Foundation for Chemical Research (SON) with financial aid from the Netherlands Organization for the Advancement of Pure Research (ZWO).

Registry No. 1 ($n = 0$), 77877-86-2; **1** ($n = 1$), 53914-89-9; **1** ($n = 2$), 86309-73-1; **1** ($n = 3$), 86309-74-2; **1** ($n = 4$), 95216-11-8; **1** ($n = 5$), 95216-12-9; **1** ($n = 6$), 95216-13-0; **2** ($n = 0$), 57624-50-7; **2** ($n = 1$), 53914-83-3; **2** ($n = 2$), 57624-51-8; **2** ($n = 3$), 57624-52-9; **2** ($n = 4$), 57659-55-9; **2** ($n = 5$), 57624-53-0; **2** ($n = 6$), 108744-27-0; **3** ($n = 0$), 14098-44-3; **3** ($n = 1$), 14098-24-9; **3** ($n = 2$), 67950-78-1; **3** ($n = 3$), 72216-45-6; **3** ($n = 4$), 63144-76-3; **3** ($n = 5$), 77963-50-9; **3** ($n = 6$), 104946-62-5.

Supplementary Material Available: Tables of all nonstandard MM2 parameters used in the calculations and coordinates, torsion angles, and steric energies of all energy-minimized conformations (21 pages). Ordering information is given on any current masthead page.

(37) N.M.C.-1280 Manual, Nicolet Magnetic Corporation, Fremont, 1982.
(38) Allinger, N. L. *QCPE-bull.* **1983**, *3*, 32-33.
(39) A complete list of all nonstandard MM2 parameters used in the calculations is with the supplementary material.
(40) Incorporated in the ChemGraf suite, by E. K. Davies, 1985, distributed by Chemical Design Ltd., Oxford.
(41) Estimate based on relative values of corresponding parameters in the AMBER force field: Weiner, S. J.; Kollman, P. A.; Nguyen, D. T.; Case, D. A. *J. Comput. Chem.* **1986**, *7*, 230-252.
(42) Uiterwijk, J. W. H. M., Harkema, S.; van der Waal, B. W.; Göbel, F.; Nibbeling, H. T. M. *J. Chem. Soc., Perkin Trans. 2* **1983**, 1843-1855.

An XPS Study of Rhodium Carbonyls Adsorbed on Planar Aluminas: Formation of Geminal Dicarbonyl Species

B. G. Frederick,[†] G. Apai,*[‡] and T. N. Rhodin[§]

Contribution from the Corporate Research Laboratories, Eastman Kodak Company, Rochester, New York 14650, and Cornell Materials Science Center, Cornell University, Ithaca, New York 14850. *Received August 25, 1986*

Abstract: The rhodium geminal dicarbonyl species has been observed to form from the evaporation of $Rh_4(CO)_{12}$ onto cooled planar aluminas under ultrahigh vacuum (UHV) conditions. The Rh 3d core level binding energies, Rh:(CO) stoichiometric ratio, and CO bonding site of the geminal dicarbonyl have been determined with X-ray photoelectron spectroscopy (XPS, ESCA). Comparisons are made with $Rh_2(CO)_4Cl_2$, $Rh_4(CO)_{12}$, and $Rh_6(CO)_{16}$ evaporated on amorphous and crystalline carbon supports at low temperatures. The instability of these rhodium carbonyls under UHV at room temperature is demonstrated; therefore, our low-temperature data permit us to correct previously reported values for Rh 3d binding energies of rhodium complexes impregnated on powder catalysts and recommend, in some cases, the species reponsible for the previously reported binding energies. We identify the Rh $3d_{5/2}$ binding energy of the geminal dicarbonyl as 310.2 eV, indicating that the electron density on the rhodium atom is comparable to Rh^{3+} compounds despite its assigned formal charge of Rh^{1+}. Reversible changes in Rh core level binding energies following repetitive treatments of vacuum and 1 atm CO exposure at room temperature indicate dispersive effects of rhodium and further demonstrate that the planar aluminas behave similarly to conventional powder alumina catalyst systems.

I. Introduction

Transition-metal carbonyl clusters supported in a variety of ways have provided a wealth of information concerning interactions among support, metal, and ligands.[1-3] Analogies have also been made that discrete molecular metal clusters may model metal surfaces in processes of chemisorption and bonding.[4] Decomposition of supported organometallic compounds has provided a

[†] Department of Chemistry, Cornell University.
[‡] Corporate Research Laboratories, Eastman Kodak Company.
[§] School of Applied and Engineering Physics, Cornell University.

(1) Zwart, J.; Snel, R. *J. Mol. Catal.* **1985**, *30*, 305.
(2) Bailey, D. C.; Langer, S. H. *Chem. Rev.* **1981**, *81*, 109.
(3) Phillips, J.; Dumesic, J. A. *Appl. Catal.* **1984**, *9*, 1.
(4) Muetterties, E. L.; Rhodin, T. N.; Brucker, C. F.; Pretzer, W. R. *Chem. Rev.* **1979**, *79*, 91.

0002-7863/87/1509-4797$01.50/0

means to prepare bare metal clusters of controllable size.[5] In addition, the study of supported organometallic compounds has the potential of providing well-defined surface species, just as the study of single crystals has provided well-defined surfaces for chemisorption studies. In a recent paper[6] we demonstrated this application of supported rhodium carbonyl clusters by using X-ray photoelectron spectroscopy (XPS). In this paper, we extend the potential of supported carbonyl clusters toward the understanding of more complicated catalytic systems. Although vibrational data are valuable in determining structural information for impregnated powder catalysts, it appears that XPS can also provide a greater understanding of bonding and the electronic properties of surface species when model catalysts are used.

The chemisorption of CO on Al_2O_3-supported Rh was first studied by Yang and Garland[7] with use of infrared techniques. The system has been further studied by a number of investigators[8-10] in an attempt to identify a carbonyl species on highly dispersed rhodium which exhibits a doublet in the carbonyl infrared (IR) spectrum, corresponding to symmetric and antisymmetric coupling between pairs of CO molecules adsorbed on the same rhodium atom. Upon the basis of comparisons with the infrared spectra of the dimers[11] $Rh_2(CO)_4Cl_2$ and $Rh_2(CO)_4Br_2$, whose structures are well known,[12] the low-coverage alumina-supported Rh species are characterized to be isolated Rh atoms with two adsorbed geminal CO molecules. In addition, extended X-ray absorption fine structure (EXAFS) data[13,14] indicate three oxide linkages from the rhodium atom to the support. This same dicarbonyl species was produced by Smith,[15] by using a different approach in which solution impregnation of $Rh_6(CO)_{16}$ onto hydroxylated alumina powders was observed to decompose into the characteristic geminal dicarbonyl IR bands. The more dehydroxylated supports showed slower production of the dicarbonyl, and Watters[16] has suggested the necessity of H_2O for the facile decarbonylation and recarbonylation of the rhodium core. XPS has been applied, in a cursory way, to both the carbonyl clusters solution impregnated on alumina powder[17] and the dispersed catalyst system[14] formed from $RhCl_3 \cdot 3H_2O$ impregnated on alumina powder to follow the electronic changes during adsorption as well as the effects of Rh dispersion.

Several of the conclusions concerning Rh oxidation states associated with these supported complexes need to be reinterpreted because of the propensity for the complexes to decompose in UHV at ambient temperature. Recently, we have shown[6] that the stability of the carbonyl ligands in these rhodium clusters under ultrahigh vacuum (UHV) at room temperature is rather poor and that stabilization at reduced temperatures is necessary if the intact clusters are to be studied and compared with other surface species. We report here the vapor deposition of $Rh_6(CO)_{16}$ and $Rh_4(CO)_{12}$ onto cold alumina supports under UHV conditions. Preparation of clean planar supports eliminated charging problems and permitted analysis of both the rhodium and the carbonyl peak intensities which cannot be accomplished in the more traditional catalyst supports due to hydrocarbon contamination and charge-referencing difficulties. Decomposition of the clusters on alumina under UHV occurs immediately and, for less than $^1/_3$ monolayer rhodium atom coverage, forms a species which we identify as the geminal dicarbonyl. To confirm this assignment, we characterized the dimer $Rh_2(CO)_4Cl_2$ evaporated on a cold amorphous carbon substrate and compared the core level binding energies for the well-characterized dimeric compound with the alumina-supported dicarbonyl species. Decomposition of the alumina-supported dicarbonyl state is observed to proceed even at reduced temperature, and the final room temperature species contains a single carbonyl ligand per Rh atom. The CO stoichiometry and binding energies we obtain for the decomposed dimer $Rh_2(CO)_2Cl_2$ at room temperature are similar to that of the alumina-supported *gem*-dicarbonyl in that a monocarbonyl ligand remains bonded to each Rh atom. Exposure of the alumina-supported decomposed dicarbonyl to CO at 1 atm flowing conditions produces a reversible state which we attribute to the dispersive effects of low-temperature CO treatments observed on high surface area powders. Intensity calculations are used to indicate the stoichiometry of the various surface species.

II. Experimental Section

Photoemission experiments were performed with a VG ESCALAB Mark II spectrometer system with a hemispherical analyzer and diffusion and titanium sublimation pumps. Pressures were typically in the low-to-mid 10^{-10} mbar range. The measurements were made with an unmonochromatized Mg Kα X-ray source. Binding energies were determined within an uncertainty of ± 0.1 eV. The system also included an attached preparation chamber equipped with sample cooling, heating, and argon ion-sputtering capabilities as well as H_2O, O_2, and CO gas-handling lines. Flowing CO treatments were performed in a high-pressure cell (1 atm) within a fast-entry lock attached to the preparation chamber.

Carbonyl Evaporation Technique. The $Rh_4(CO)_{12}$ and $Rh_6(CO)_{16}$ clusters were obtained from Strem Chemical; $Rh_2(CO)_4Cl_2$ was prepared from literature methods[18] and characterized by IR spectroscopy. The carbonyl compounds were all stored under CO and kept refrigerated to prevent decomposition. The carbonyls were evaporated from a gold-coated molybdenum heater with a stainless-steep cap to direct the evaporation of the carbonyl powder toward the cooled substrate. The substrate was cooled below 170 K before evaporation but may have warmed slightly during transfer into the analysis chamber where it was again kept cold. The $Rh_4(CO)_{12}$ was evaporated at room temperature for $\sim$1 min in UHV, yielding a reproducible coverage of one-to-two equivalent Rh atom monolayers, or for 15 s for a coverage of $\sim^1/_3$ of a monolayer (3×10^{14} atm Rh/cm^2). $Rh_6(CO)_{16}$ was evaporated between 100 and 115 °C but was monitored by the chamber pressure during evaporation. Some outgassing during heating prevented the $Rh_6(CO)_{16}$ from being deposited as cleanly as the $Rh_4(CO)_{12}$, as noted by an increase in the carbonaceous carbon 1s peak. For this reason, we used $Rh_4(CO)_{12}$ to investigate the formation of the geminal dicarbonyl, since carbon-to-rhodium intensity ratios needed to be calculated as accurately as possible.

Substrate Preparation. The carbon substrate was chosen as a weakly interacting support and was prepared from a high-purity graphite sheet by Ar^+ sputtering at 3–5 kV to reduce contaminants to detection limits. This surface treatment forms a well-characterized amorphous carbon surface. This is substantiated by nucleation and electronic structure studies of small metal particles.[19,20] Planar alumina films were obtained from commercial aluminum foils. The $\sim$30 Å thick native oxide was degreased with acetone, sputtered lightly (1 kV Ar^+, 1 min, 6 μA beam current) to remove hydrocarbon contaminants reducing the film to $\sim$20 Å, and heat cleaned to 673 K under a 2×10^{-6} mbar O_2 or H_2O environment to burn off hydrocarbons. During the burn off, the surface reoxidized to a 30 Å thick film, as calculated from XPS Al^{3+} and Al^0 peak intensities. The remaining carbonaceous carbon was small enough to allow a background subtraction from the carbonyl C 1s spectra. For purposes of comparing the differences in interactions of $Rh_4(CO)_{12}$ with either H_2O or O_2 treated alumina surfaces we prepared some aluminas by oxidizing clean aluminum surfaces in UHV. These thin-film aluminas were prepared by sputtering 0.25 mm 5 N aluminum foil (Alpha Chemical) until the Al^{3+} 2p and O 1s XPS lines were reduced to the detection limit and then oxidized with high-purity O_2 or H_2O to produce an un-

(5) Legare, P.; Sakisaka, Y.; Brucker, C. F.; Rhodin, T. N. *Surf. Sci.* **1984**, *139*, 316.
(6) Apai, G.; Frederick, B. G. *Langmuir* **1987**, *3*, 395.
(7) Yang, A. C.; Garland, C. W. *J. Chem. Phys.* **1957**, *61*, 1504.
(8) Yao, H. C.; Rothschild, W. G. *J. Chem. Phys.* **1978**, *68*, 4774.
(9) Rice, C. A.; Worley, S. D.; Curtis, C. W.; Guin, J. A.; Tarrer, A. R. *J. Chem. Phys.* **1981**, *74*, 6487.
(10) Yates, J. T.; Duncan, T. M.; Worley, S. D.; Vaughan, R. W. *J. Chem. Phys.* **1979**, *70*, 1219.
(11) Garland, C. W.; Wilt, J. R. *J. Chem. Phys.* **1962**, *36*, 1094.
(12) Dahl, L. F.; Martell, C.; Wampler, D. L. *Inorg. Chem.* **1961**, *83*, 1762.
(13) van't Blik, H. F. J.; van Zon, J. B. A. D.; Huizinga, T.; Vis, J. C.; Koningsberger, D. C.; Prins, R. *J. Phys. Chem.* **1983**, *87*, 2264.
(14) van't Blik, H. F. J.; van Zon, J. B. A. D.; Huizinga, T.; Vis, J. C.; Koningsberger, D. C.; Prins, R. *J. Am. Chem. Soc.* **1985**, *107*, 3139.
(15) Smith, A. K.; Hugues, F.; Theolier, A.; Basset, J. M.; Ugo, R.; Zanderighi, G. M.; Bilhou, J. L.; Bilhou-Bougnol, V.; Graydon, W. F. *Inorg. Chem.* **1979**, *18*, 3104.
(16) Watters, K. L.; Howe, R. F.; Chojnacki, T. P.; Fu, C.-M.; Schneider, R. L.; Wong, N.-B. *J. Catal.* **1980**, *66*, 424.
(17) Andersson, S. L. T.; Watters, K. L.; Howe, R. F. *J. Catal.* **1981**, *69*, 212.
(18) McCleverty, J. A.; Wilkinson, G. *Inorg. Synth.* **1966**, *8*, 211.
(19) Mason, M. G.; Lee, S.-T.; Apai, G. *Chem. Phys. Lett.* **1980**, *76*, 51.
(20) Egelhoff, W. F., Jr.; Tibbetts, G. C. *Phys. Rev.* **1979**, *B19*, 5028.

hydroxylated or hydroxylated amorphous alumina, respectively. Oxidation was performed under flowing conditions at pressures of 1×10^{-6} mbar for 1000 L exposure at 373 K and at 673 K to produce a more crystalline surface. The oxidation produced a film thickness of ~8–10 Å, calculated from XPS Al^{3+} and Al^0 intensities. Planar aluminas produced by the above methods offer the advantage of referencing XPS spectral features to the aluminum metal 2p peaks and of greatly reducing inhomogeneous charging problems. No broadening or shifting of the spectral features due to charging was observed, and good agreement was obtained between the binding energies for initial deposition of the carbonyl clusters on the graphite and the alumina surfaces. We were also able to distinguish the method of wet (H_2O) oxidation from dry (O_2) oxidation by analyzing the XPS O 1s peak line shape, which is considerably more asymmetric in the hydroxylated alumina than in the unhydroxylated alumina, as Johnson[21] describes. Electron loss spectra, which are particularly sensitive to oxide environment, were initially used to compare our data with the data of Johnson; however, the method was not used routinely to characterize samples prior to carbonyl deposition because of the possibility that electron beam damage might produce surface defects.

XPS Data Analysis. Referencing of the X-ray data was done by assigning the C 1s binding energy to 284.4 eV for the amorphous carbon substrate. On the alumina substrates, the Al^0 2p binding energy was assigned to 72.7 eV. These values yielded consistent binding energies for the carbonyl peaks and the initial low-temperature rhodium-binding energies for carbon and high coverages on aluminas, demonstrating that charging on the planar aluminas does not occur. The 2p peak attributable to Al^{3+} was not a good reference, especially if the alumina was ultrathin, as the binding energy varied with the surface preparation, and the splitting between the Al^{3+} and Al^0 2p core levels varied by as much as 1.5 eV. The differences in Al^{3+} 2p binding enegies may be attributed to variations in the stoichiometry of the aluminum oxide as has been discussed previously.[22]

Calculations of rhodium coverage were performed by using Scofield's[23] theoretical cross sections and accounting for an analyzer transmission function inversely proportional to the square root of the kinetic energy of the emitted photoelectron. The asymmetry parameter, β, was incorporated into the cross sections when comparing orbitals of different symmetry.[24] Alumina film thicknesses were based on a mean free path of 24.2 Å in aluminum metal and 20.7 Å in alumina for an 1180-eV electron.[21,25]

Peak areas were determined by numerical integration of the raw data by using linear backgrounds, and deconvolution was performed with the Gaussian peak synthesis programs accompanying the Vacuum Generators instrument.

III. Results and Discussion

A. Characterization of Supported Carbonyl Clusters. Before examining the reactivity of $Rh_4(CO)_{12}$ on alumina, we established the binding energies of several intact carbonyl clusters on the surface, which could then be compared with species observed in the decomposition of $Rh_4(CO)_{12}$. While several workers[17,26,27] have suggested that rhodium carbonyls are decomposed by the X-ray beam, we find no evidence for this conclusion. At 210 K on the carbon substrate, $Rh_6(CO)_{16}$ showed no change in binding energy over a 2–3 h period, while at room temperature decomposition occurred much more rapidly. Nevertheless, over a 10–12 h period under UHV at low temperatures, with or without the X-ray beam, the metal carbonyls were observed to decarbonylate.

1. $Rh_4(CO)_{12}$ and $Rh_6(CO)_{16}$ on Carbon Substrates. Evaporation of $Rh_4(CO)_{12}$ and $Rh_6(CO)_{16}$ onto cold carbon supports has been shown by us previously[6] to be essentially intact; the characterization of the bridging and terminal CO ligand binding energies are in agreement with chemisorption studies of CO on Rh(111) and Rh(331) surfaces,[28] and the stoichiometries we obtained from XPS line-intensity ratios are consistent with expected ratios for intact clusters. The binding energies of the O 1s and C 1s core levels for terminal and bridging CO are summarized in Table I, along with the Rh $3d_{5/2}$ binding energy for each system. For reference, in Figure 1 we show the Rh 3d peaks for $Rh_6(CO)_{16}$, $Rh_4(CO)_{12}$, and $Rh_2(CO)_4Cl_2$, vapor deposited on carbon, and for a clean Rh(111) single crystal. The full-width at half maximum (FWHM) of 1.2 eV is much narrower than previously reported XPS data for the carbonyls[14,17,26,27] and indicates the integrity of the clusters and that inhomogeneous charging is not a problem.

The shift of the rhodium core levels in the cluster complexes to higher binding energy has been attributed to several factors;[29] electron withdrawal of the CO ligands and initial and final state effects in the transition from the bulk metal to the cluster state. The binding energy shift related to particle size has been shown to be dominated by initial state effects for systems of this type.[30,31]

Table I. Carbonyl Species Binding Energy

		terminal		bridging	
Rh system	Rh $3d_{5/2}$	O 1s	C 1s	O 1s	C 1s
Rh(111)[a]	307.1	532.1	286.1	530.7	285.3
Rh(331)[a]	307.1	532.1	286.1	531.2	~286.1
$Rh_6(CO)_{16}$/C	309.45	534.1	287.6	532.1	*b*
$Rh_4(CO)_{12}$/C	309.5	534.2	~287.9	532.7	*b*
$Rh_2(CO)_4Cl_2$/C	309.7	534.2	288.1	none	none
$Rh_6(CO)_{16}$/Al ox	309.45	534.2	287.8	*b*	286.7
$Rh_4(CO)_{12}$/Al ox	309.5	534.1	288.1	*b*	287.4
$Rh(CO)_2$/Al ox	310.2	534.2	288.4	none	none

[a] Data from ref 28. [b] Peak obscured by substrate core level.

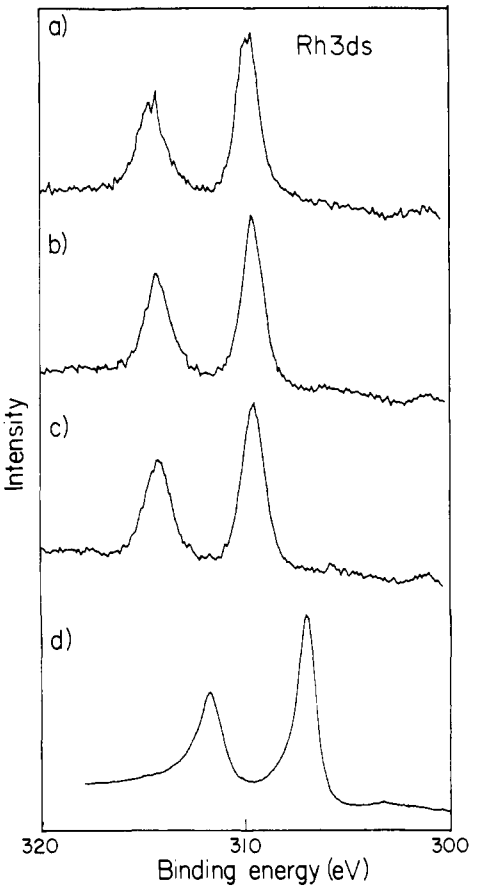

Figure 1. Rh $3d_{5/2}$ and $3d_{3/2}$ core level spectra for (a) $Rh_2(CO)_4Cl_2$ (BE = 309.7 eV), (b) $Rh_4(CO)_{12}$ (BE = 309.5 eV), and (c) $Rh_6(CO)_{16}$ (BE = 309.45 eV) evaporated on cold amorphous carbon supports and (d) Rh(111) 3d core levels (BE = 307.1 eV). All FWHMs are 1.2 eV.

(21) Johnson, E. Thesis, Cornell University, 1985.
(22) Wagner, C. D.; Six, H. A.; Jansen, W. T.; Taylor, J. A. *Appl. Surf. Sci.* **1981**, *9*, 203.
(23) Scofield, J. H. *J. Electron Spectrosc. Relat. Phenom.* **1976**, *8*, 129.
(24) Reilman, R. F.; Msezane, A.; Manson, S. T. *J. Electron. Spectrosc. Relat. Phenom.* **1976**, *8*, 389.
(25) Penn, D. R. *J. Electron. Spectrosc. Relat. Phenom.* **1976**, *9*, 29.
(26) Batista-Leal, M.; Lester, J. E.; Lucchesi, C. A. *J. Electron Spectrosc. Relat. Phenom.* **1977**, *11*, 333.
(27) Andersson, S. L. T.; Scurrell, M. S. *J. Catal.* **1979**, *59*, 340.
(28) DeLouise, L. A.; White, E. J.; Winograd, N. *Surf. Sci.* **1984**, *147*, 252.
(29) Apai, G.; Lee, S.-T.; Mason, M. G.; Gerenser, L. J.; Gardner, S. A. *J. Am. Chem. Soc.* **1979**, *101*, 6880.
(30) Mason, M. G. *Phys. Rev. B* **1983**, *27*, 748.

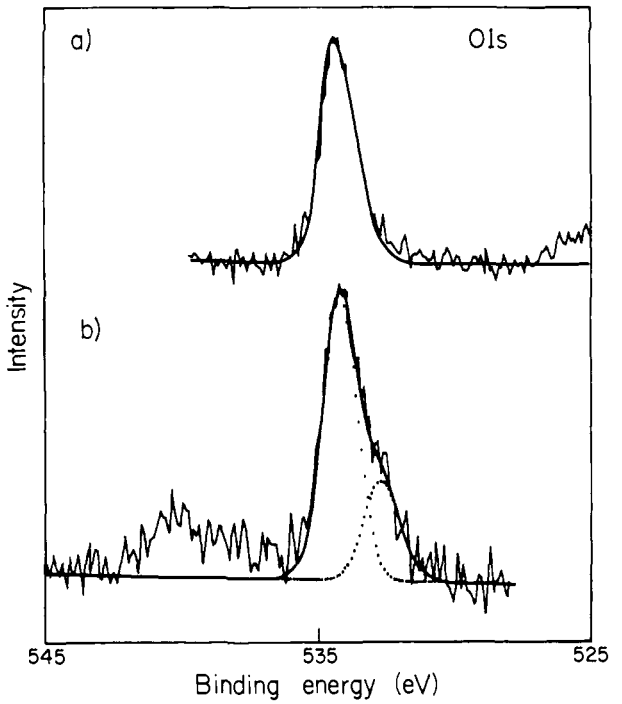

Figure 2. O 1s core-level spectra for (a) $Rh_2(CO)_4Cl_2$, and (b) $Rh_4(CO)_{12}$ evaporated on cold carbon supports showing terminal CO at 534.2 eV and edge bridging at 532.7 eV (FWHM = 1.6 eV).

Mason[30] shows that, for bare metal clusters on weakly interacting carbon substrates, the final state relaxation is on the order of −0.5 eV but is dominated by initial state shifts of +2 eV, producing a net increase in the binding energy. The number of like nearest neighbors is important in the rehybridization of the d orbitals; X-ray absorption spectroscopy data[32] and results of self consistent field (SCF) calculations support this view.[31]

2. $Rh_2(CO)_4Cl_2$ on Carbon Substrates. Figure 2 compares the O 1s core levels of $Rh_2(CO)_4Cl_2$ with $Rh_4(CO)_{12}$ evaporated on cold graphite substrates, fit with gaussians of FWHM of 1.6 eV. The O 1s peak in $Rh_2(CO)_4Cl_2$ indicates only one geminal CO binding site, as would be expected. Figure 3 shows the Cl 2p doublet fit with a FWHM of 1.1 eV, a spin-orbit splitting of 1.6 eV, and a $2p_{3/2}$:$2p_{1/2}$ ratio of 1.8:1.[33] The Cl $2p_{3/2}$ binding energy of 199.4 eV agrees well with reported values for bridging chloride ligands in clusters with metal–metal bonds,[34-36] where both bridging and terminal chlorides are present and differ in binding energy by ~1 eV. The chlorine doublet deconvolution into only one binding site (bridging) is an indication of the integrity of the dimer's framework at low temperature. The stoichiometry for $Rh_2(CO)_4Cl_2$ is calculated as described above to be 2.0:(2.8 ± 0.6):2.2 as compared to the expected values of 2:4:2. This represents a CO loss of ~25% during deposition, which is evidence of the instability of the CO ligands under UHV and is consistent with CO losses for low coverages of $Rh_4(CO)_{12}$ on cold carbon.[6] Due to CO loss, our value of 309.7 eV must be considered a lower limit due to the electron-withdrawing nature of CO ligands.

Upon warming to room temperature under UHV conditions, the Rh binding energy shifted from 309.7 to 308.6 eV, while the stoichiometry became 2.0:1.9:2.2, indicating that significant decarbonylation has occurred. Formation of a $Rh_2(CO)_2Cl_2$ species under UHV conditions seems probable by analogy to the more traditionally prepared powder alumina-supported Rh(CO) monocarbonyl species[10,39] and the Rh(NO) mononitrosyl species[37]

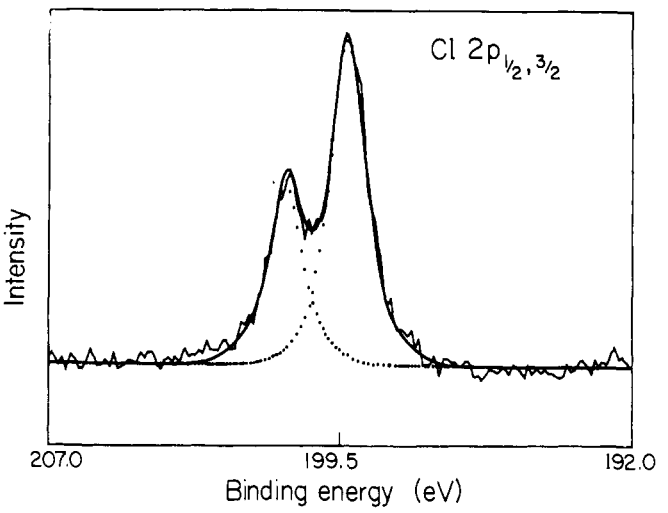

Figure 3. The Cl 2p doublet for $Rh_2(CO)_4Cl_2$ shows only one chloride bonding site, fit with a FWHM = 1.1 eV, a spin-orbit splitting of 1.6 eV, and a $2p_{3/2}$:$2p_{1/2}$ ratio of 1.8.

identified from IR data upon loss of CO and NO, respectively, after evacuation. The Rh 3d binding energy for the decomposed dimer of 308.6 eV is the same value as previously reported by van't Blik et al.,[14] which implies that the species they observed with XPS at room temperature under UHV conditions were most likely partially decarbonylated and not the intact $Rh_2(CO)_4Cl_2$ dimer that they investigated with EXAFS and other techniques. Nefedov et al.[38] report, without indication of temperature, a value of 309.2 eV for the Rh $3d_{5/2}$ level of $Rh_2(CO)_4Cl_2$, which is also probably partially decomposed. Primet et al.[39] report very low values of 307.8 eV for a geminal carbonyl complex on zeolites at room temperature. The discrepancies lead us to believe that extreme care must be taken to compare chemical states of species with use of different techniques.

3. $Rh_4(CO)_{12}$ and $Rh_6(CO)_{16}$ on Alumina. We previously discussed[6] the evaporation of 1–3 monolayer equivalent Rh atom coverages of $Rh_4(CO)_{12}$ and $Rh_6(CO)_{16}$ onto UHV-prepared alumina films. The Rh 3d binding energy upon initial deposition at low temperature was 309.5 and 309.45 eV, respectively, which agreed to within 0.05 eV, with the results on cold graphite substrates. The presence of both terminal and bridging CO ligands (edge and face) was easily determined from the O 1s core spectrum, which shows that metal aggregates of at least three atoms were retained on the cooled surface. After warming to room temperature, decarbonylation was observed, with a decrease in the Rh binding energy. Exposure to 1 atm CO did not indicate recarbonylation or dispersion effects, which is in agreement with the observations of others[7,8,10] that coverages low enough to prevent metal–atom aggregation are necessary for the formation of the monodispersed dicarbonyl.

For low coverage deposition of $Rh_4(CO)_{12}$, two alumina substrates were prepared. The aluminum surface native oxide was gently sputtered and heat cleaned with pure, dry O_2 in one case and H_2O in the other, producing 32–34 Å thick planar aluminas. The evaporation of $<^1/_4$ monolayer equivalent Rh atom coverage of $Rh_4(CO)_{12}$ at temperatures below 170 K produced on both substrates a species with a Rh $3d_{5/2}$ binding energy of 310.2 eV with a FWHM of 1.3 eV (Figure 4). The C 1s regions, shown in Figure 5, indicate only *one* carbonyl carbon peak at 288.4 eV (FWHM = 1.7 eV), although for the O_2 treated alumina a second carbon peak at 284.8 eV is observed, which is typical of carbonaceous carbon. Calculations of the carbonyl carbon and rhodium peak areas result in a CO:Rh ratio of 1.9:1. This loss of CO ligands occurred within 10 min, and further decarbonylation at

(31) Parmigiani, F.; Kay, E.; Bagus, P. S.; Nelin, C. J. *J. Electron Spectrosc. Relat. Phenom.* **1985**, *36*, 257.
(32) Balerna, A.; Bernieri, E.; Picozzi, P.; Reale, A.; Santucci, S.; Burattini, E.; Mobilio, S. *Phys. Rev. B* **1985**, *31*, 5058.
(33) Theoretical values of 1.95 (ref 23) and experimental values of 1.9 ± 0.2 (ref 34) have been previously reported for the Cl $2p_{3/2}$:$2p_{1/2}$ ratio.
(34) Hamer, A. D.; Walton, R. A. *Inorg. Chem.* **1976**, *13*, 1446.
(35) Tisley, D. G.; Walton, R. A. *Inorg. Chem.* **1973**, *12*, 373.
(36) Nefedov, V. I. *J. Electron Spectrosc. Relat. Phenom.* **1977**, *12*, 459.
(37) Liang, J.; Wang, H. P.; Spicer, L. D. *J. Phys. Chem.* **1985**, *89*, 5840.
(38) Nefedov, V. I.; Shubochkina, E. F.; Kolomnikov, I. S.; Baranovskii, I. B.; Kukolev, V. P.; Golubnichaya, M. A.; Shubochkin, L. K.; Porai-Koshits, M. A.; Vol'pin, M. E. *Russ. J. Inorg. Chem.* **1973**, *18*, 444.
(39) Primet, M.; Vedrine, J. C.; Naccache, C. *J. Mol. Catal.* **1978**, *4*, 411.

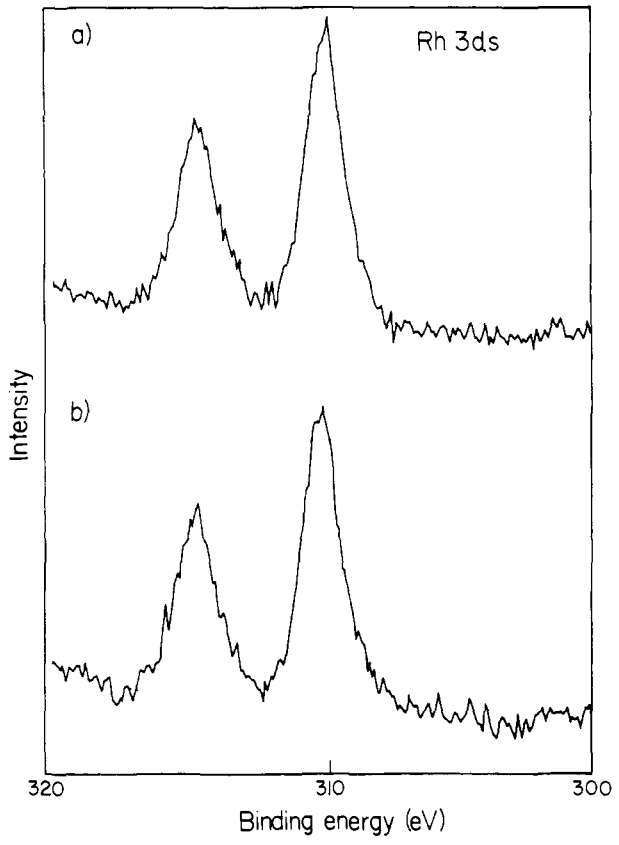

Figure 4. Rh 3d peaks for the geminal dicarbonyl, $Rh(CO)_2$, formed on 32–34 Å thick oxides cleaned and annealed at 673 K with (a) 1×10^{-6} mbar H_2O and (b) 1×10^{-6} mbar O_2. Evaporation of less than $^1/_4$ monolayer $Rh_4(CO)_{12}$ was done with the substrate temperature below 173 K.

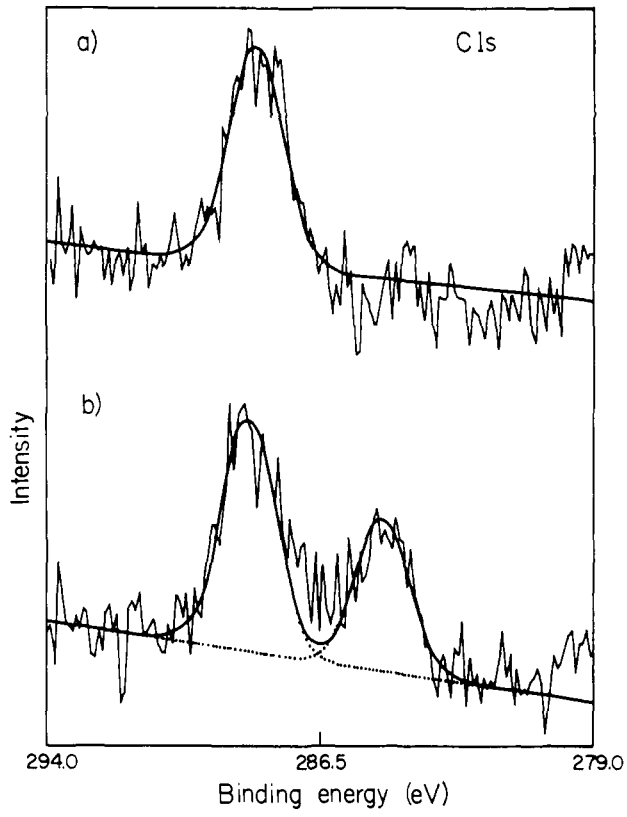

Figure 5. C 1s spectra for the formation of the geminal dicarbonyl, $Rh(CO)_2$, from evaporation of $^1/_4$ monolayer equivalent Rh atom coverage of $Rh_4(CO)_{12}$ at 160 K on (a) air-oxidized aluminum foil cleaned (1 min, 1 kV Ar^+) and annealed in H_2O (673 K, 2×10^{-6} mbar) and (b) air-oxidized aluminum foil cleaned and annealed in O_2. Background carbon prior to evaporation of the carbonyl clusters has been subtracted. The carbonyl carbon peaks at 288.4 eV are fit with a 1.7 eV FWHM. The second peak in spectrum (b) is attributed to carbonaceous carbon at 284.8 eV.

temperatures of 150 K resulted in a decrease in Rh 3d binding energies of several tenths of an electron volt per half hour, with decreasing CO:Rh ratios. Considering the coverage dependence known for the formation of the dicarbonyl, the high-binding energy of 310.2 eV, and the instability under UHV conditions, we identity this species as the monodispersed rhodium geminal dicarbonyl. The final room temperature species had a Rh BE of 308.3 eV and a Rh:CO ratio of 1.0:1.0. For low coverages, exposure to 1 atm/35 sccm flowing CO in situ produced a reversible Rh binding-energy shift from 308.3 to 308.6 eV. Cycles of treatment with 1 atm CO and decarbonylation at room temperature could be repeated several times with the Rh BE shifting between 308.6 and 308.3 eV. No significant increase in adsorbed CO was measured; however, our cooling capabilities of ~210 K in the 1 atm cell and the lack of continuous cooling for several minutes during transfer probably were not sufficient to stabilize the dicarbonyl. The dispersive effects known[8,10] for CO exposure probably account for the change in binding energy of the Rh 3d core levels from a $Rh_n(CO)_n$ cluster to a monodispersed Rh(CO) species, similar to that observed during decomposition of $Rh_2(CO)_4Cl_2$. Further, the reversibility of the carbon monoxide treatment suggests that the rhodium carbonyl species produced on 30 Å planar alumina films behave like those produced on high surface area powders studied by others.[10,14] Finally, the Rh 3d binding energy of 308.6 eV, identified as a monodispersed Rh(CO) species, indicates that the dicarbonyl species prepared on high surface area powders by van't Blik et al.[14] had decomposed under UHV.

B. Consideration of Rhodium Carbonyl Binding Energies. Core-level binding energies have been important in the identification of oxidation states for surface species. Binding energies[17] for Rh^{1+} compounds have been reported in the range of 307.6–309.6 eV with a mean of 308.8 eV, while Rh^{3+} compounds have been reported as 308.8–311.3 eV with a mean of 310.3 eV. While the formal charge in the dimer $Rh_2(CO)_4Cl_2$ is Rh^{1+}, our assignment of the Rh $3d_{5/2}$ core level to 309.7 eV (as a *lower* limit) is high for a 1+ species. The rhodium carbonyls, $Rh_4(CO)_{12}$ and $Rh_6(CO)_{16}$, also have consistently high-binding energies of 309.5 and 309.45 eV, respectively, despite their formal Rh^0 oxidation state. Although it may be fortuitous, Andersson et al.[17] report a value of 309.3 eV for a species with IR characteristics of $Rh_6(CO)_{16}$. The high rhodium binding energies for all of the intact carbonyl clusters can be understood in light of the backbonding model for CO ligands, in which σ donation from the CO 5σ MO to the metal is offset of π backbonding from the metal back into the CO $2\pi^*$ MO, resulting in a net charge transfer away from the metal. This depletion of charge on the rhodium atoms would predict the observed increase in the Rh BE vs. that of bare clusters. Further consideration of a 310.2 eV binding energy assignment to the dicarbonyl leads to several conclusions: (1) Examination of the sequence of binding energies for the Rh_6, Rh_4, and Rh_2 initially deposited clusters as a function of metal–metal bonds per rhodium atom would indicate that the Rh binding energy for the geminal dicarbonyl should be higher than 309.7 eV. (2) Comparing the structure of $Rh_2(CO)_4Cl_2$ with the structure proposed by van't Blik et al.[14] from EXAFS data for the geminal dicarbonyl (see Figure 6), the differences are the substitution of three oxide linkages for the two chloride ligands and the one metal–metal bond. Initial and final state effects associated with the metal–metal bond would suggest that the dimer would not have as high a binding energy as the monodispersed geminal dicarbonyl species. (3) If the binding energy of 310.2 eV is accepted for the geminal dicarbonyl, then some reconsideration of the formal charge assignment[10,14] of Rh^{1+} may be in order because previous verification of Rh^{1+} based upon XPS analysis must be considered erroneous. Indeed, electron spin resonance (ESR) data[14] show no signal for the dicarbonyl state, indicating either Rh^{1+} or Rh^{3+} (but not Rh^{2+}). The dependence of the IR carbonyl-stretching frequencies on the

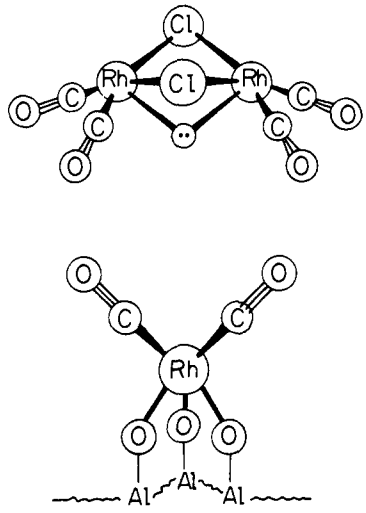

Figure 6. A comparison of the structure of the geminal dicarbonyl species and $Rh_2(CO)_4Cl_2$. Adapted from ref 10 and 12. The symbol ⊙ represents a bent Rh–Rh bond.

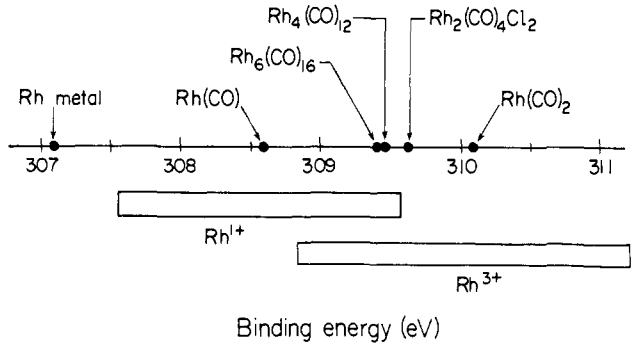

Figure 7. Diagram showing the comparison of carbonyl cluster Rh $3d_{5/2}$ binding energies with Rh^{1+} and Rh^{3+} binding energy regions.

metal–atom charge indicates that the monodispersed dicarbonyl is electronically similar to the $Rh_2(CO)_4Cl_2$ dimer. The frequencies of the monodispersed dicarbonyl are, however, slightly higher, indicating that the rhodium atom in the monodispersed geminal dicarbonyl is more positive than in the dimer,[38] which correlates with our observed XPS binding energies. As we have pointed out, however, the binding energy for all of these intact Rh^0 and Rh^{1+} carbonyls are very high, comparable to Rh^{3+} compounds. For example, the Rh $3d_{5/2}$ binding energy for $RhCl_3 \cdot 3(H_2O)$ is reported at 309.7 eV,[38] and we find a binding energy of 310.2 eV for Rh_2O_3.[40] Although the similarity in the IR data between the dimer and the monodispersed dicarbonyl suggests that the environment of the Rh atom is similar, what has not been previously suspected is that the binding energy for Rh in all of these carbonyl clusters is very high. Despite formal assignments of Rh^0 and Rh^{1+}, the electron density on the rhodium cluster framework is deficient, comparable to other Rh^{3+} compounds. We, therefore, suggest that the electron density on the rhodium in the carbonyl clusters might be considered more appropriately as being electronically similar to Rh^{3+} compounds such as Rh_2O_3 and $RhCl_3 \cdot 3(H_2O)$. A comparison of these cluster-binding energies with the binding energy regions[17] attributable to Rh^{1+} and Rh^{3+} is shown in Figure 7.

Having established the binding energies of a number of surface species, several trends can be seen. The data of Table I are presented in graphical form in Figure 8. The core level O 1s and C 1s binding energies for terminal and bridging CO are plotted for the various cluster and single-crystal systems studied. In all cases, the splitting between terminal and bridging CO core levels is greater for O 1s than for C 1s. We have discussed this previously[6] in terms of initial-state effects via backbonding contributions. In all systems the binding energies for CO bonding sites are the largest for terminal CO and decrease in the order: terminal > edge-bridging (twofold site) > face-bridging (threefold site). Comparing the terminal core levels as a function of cluster size, the O 1s binding energies appear to be independent of the number of metal atoms, while the C 1s binding energies decrease monotonically with increasing cluster size, which is in the direction approaching the bulk metal system. The observation that the splittings for both O 1s and C 1s core levels between terminal and edge-bridging CO in $Rh_4(CO)_{12}$ are nearly identical with the values for CO on Rh(111)[28] suggests that the splittings may also be independent of cluster size, even though for the C 1s core levels the absolute binding energies shift with decreasing size. While these effects are enticing, further speculation as to the importance of initial and final state effects must be postponed until theoretical calculations can be performed on this system.

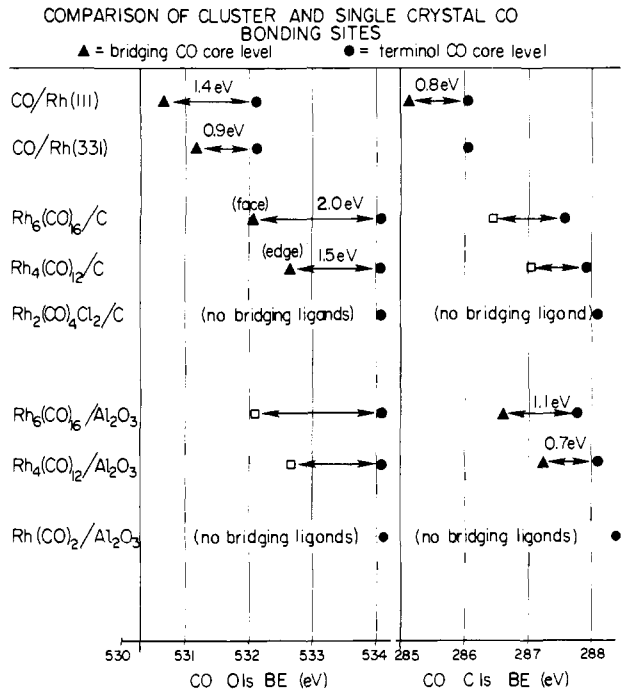

Figure 8. Comparison of O 1s and C 1s core level binding energies for terminal and bridging CO species on various clusters and single crystals. Triangles represent bridging core levels, and filled circles indicate terminal core levels. Levels that were obscured by large substrate peaks are indicated by open squares; however, the binding energies are assigned as though the splittings are identical for both substrates.

C. Alumina Surface Differences. The treatment of the alumina had no apparent effect on the initial formation of the dicarbonyl; however, comparison of the carbon spectra showed distinct differences. Subtraction of the C 1s spectrum for the H_2O-treated alumina prior to carbonyl evaporation from the C 1s spectrum after deposition of $Rh_4(CO)_{12}$ showed an increase only in carbonyl carbon attributed to the geminal CO bonding site (see Figure 5). However, for the O_2-treated alumina, a similar subtraction showed both geminal carbonyl carbon and a significant increase in carbonaceous carbon. From peak intensity calculations, the ratio of the total increase in the two carbon peaks to the intensity of the rhodium peak is ~3:1, in agreement with the stoichiometry of the original $Rh_4(CO)_{12}$ precursor. The increase in carbonaceous carbon on the O_2-treated alumina indicates that as the CO:Rh ratio decreases from 3:1 for $Rh_4(CO)_{12}$ to 2:1 for the dicarbonyl, the excess CO ligands are dissociating on the surface, while on the H_2O-treated surface, loss of CO must be occurring through molecular desorption. Two possible differences between the two alumina surfaces are the following: (1) the formation of hydroxyl groups at, or more efficient healing of, unsaturated defect sites in the sputtered alumina lattice by H_2O than by O_2; and (2) more vigorous oxidation of aluminum metal, which can diffuse into the oxide from the metal during heat treatment at 673 K, by H_2O than by O_2.[21]

(40) Gysling, H. J.; Monnier, J. R.; Apai, G. *J. Catal.* **1987**, *103*, 407.

A test of the sites responsible for CO ligand dissociation involved the use of oxide films formed totally in UHV. Evaporation of $Rh_4(CO)_{12}$ onto 8–10 Å thin film aluminas, prepared by oxidation of aluminum metal with either H_2O or O_2, showed a significant increase in the Al^{3+}/Al^0 ratio after deposition of the carbonyl. Since these aluminas could be prepared entirely under UHV conditions, carbon contamination was eliminated, and background subtraction was not necessary. However, a carbonaceous carbon peak always accompanied the carbonyl peak, and calculation of the ratio of total carbon present on the surface to rhodium coverage showed that the total carbon did not exceed the CO:Rh ratio of the original carbonyl. The coincidence of these two factors would tend to indicate that aluminum metal migrating through the 10 Å thin oxide films would account for the observed CO bond scission. Johnson[21] has shown that UHV preparation of oxides from the oxidation of aluminum metal at temperatures above 625 K results in Al^0 throughout the oxide, while aluminum migration is limited by 30 Å of oxide at temperatures below 600 K. He has also shown that H_2O is a more vigorous oxidant than O_2; thus, oxidation of Al^0 to Al^{3+} by H_2O could eliminate metal defects near the oxide surface. Thus, in the reoxidation of the sputtered native oxide at 373 K, aluminum metal migrates into the oxide until the 30-Å thickness is obtained. The difference between the O_2 and H_2O treatments in Figure 5 is that H_2O oxidizes Al^0 defects near the surface much more effectively than oxygen. As a check that uncoordinated aluminum oxide sites possibly produced by argon sputtering were not responsible, $Rh_4(CO)_{12}$ was evaporated onto a sputtered native alumina with an oxide thickness of 24 Å, as calculated from Al^{3+}:Al^0 2p core-level intensity ratios. This oxide was *not annealed*, and background subtraction of the carbon spectrum did not show an increase in carbonaceous carbon, while the geminal dicarbonyl was formed as before. Thus, we suspect that interstitial aluminum atoms, and not coordinately unsaturated sites, were responsible for the dissociative decomposition of the carbonyl on the O_2 annealed aluminas.

IV. Conclusions

Vacuum deposition of $Rh_4(CO)_{12}$ onto specially prepared planar aluminas has shown behavior similar to high surface area powder catalysts prepared through traditional impregnation techniques. The advantages of planar oxide supports and the vapor deposition of the rhodium carbonyl onto cooled substrates have allowed analysis of both the carbonyl and the rhodium XPS core levels as well as determinations of cluster stoichiometry. The rhodium geminal–dicarbonyl species, $Rh(CO)_2$, has been prepared from $\leq 1/3$ monolayer equivalent Rh atom coverage of $Rh_4(CO)_{12}$ on planar aluminas. A Rh $3d_{5/2}$ binding energy of 310.2 eV has been determined, with a Rh:CO stoichiometry of 1:2 from peak intensity calculations. At higher coverages the dicarbonyl is not formed. The Rh 3d binding energies for $Rh_2(CO)_4Cl_2$, $Rh_4(CO)_{12}$, and $Rh_6(CO)_{16}$ evaporated on carbon supports confirm the high-binding energy observed for the dicarbonyl species and show that in previous XPS studies[14,17,38,39] of these carbonyl clusters, the CO ligands have not been stabilized. The high-binding energy for the monodispersed dicarbonyl shows that, like the other carbonyl clusters studied, the electron density on the rhodium atom is decreased, comparable to Rh^{3+} compounds such as $RhCl_3 \cdot 3(H_2O)$ or Rh_2O_3. ESR data[14] determined only that the species is 1+ or 3+ (and not 2+), and hence the question of the rhodium oxidation state is reopened. We can say with certainty that the use of previous XPS results on catalyst powders run at room temperature to confirm the Rh^+ oxidation state is misleading. Decarbonylation of the dicarbonyl species proceeds rapidly under UHV conditions with a final Rh 3d binding energy of 308.3 eV and a Rh:CO ratio of 1:1. Treatment under 1 atm flowing conditions results in a redispersion of the metal as evidenced by a reversible shift in the Rh 3d BE to 308.6 eV, which we attribute to a monodispersed species on alumina. Careful investigation of the carbonyl core-level spectra has shown that the splitting between terminal and bridging positions is greater for O 1s than C 1s core levels. The terminal O 1s binding energies are independent of cluster size, while C 1s binding energies decrease with increasing cluster size.

The oxide films prepared from UHV cleaned aluminum metal are known to contain metal defects and show strenuous activity toward the carbonyl clusters, such that comparison with bulklike powder aluminas is tenuous at best. On the other hand, while the alumina surfaces prepared from the native 30-Å oxide, sputtered and annealed in H_2O, may in some ways differ from bulk powders, we feel that the similarities between the two systems are strong enough that the planar aluminas can provide significant advantages and insights into the reactivity of these carbonyl clusters on the morphologically more complicated powders.

We, therefore, have shown that planar aluminas, appropriately prepared, exhibit behavior similar to high surface area powders without the problems of inhomogeneous charging and referencing. Further, by careful preparation under UHV and low-temperature conditions, analysis of the carbonyl core levels has made it possible to determine the stoichiometries of supported species and trends in the electronic structure of supported carbonyl clusters.

Acknowledgment. Support from the Cornell Materials Science Center, Eastman Kodak Company, and NSF-DMR-83-03742 is gratefully acknowledged. Discussions with Professor R. P. Merrill and Dr. Erik Johnson were also very helpful. We thank Dr. H. Gysling for preparation and characterization of $Rh_2(CO)_4Cl_2$.